

Improved cycling stability of nanostructured electrode materials enabled by prelithiation

Liqiang Mai^{a)}

State Key Laboratory of Advanced Technology for Materials Synthesis and Processing, School of Materials Science and Engineering, Wuhan University of Technology, Wuhan, 430070 China; and Department of Chemistry and Chemical Biology, Harvard University, Cambridge, Massachusetts 02138

Lin Xu, Bin Hu, and Yanhui Gu

State Key Laboratory of Advanced Technology for Materials Synthesis and Processing, School of Materials Science and Engineering, Wuhan University of Technology, Wuhan, 430070 China

(Received 16 December 2009; accepted 23 February 2010)

This review represents recent research on using chemical prelithiation to improve cycling performance of nanostructured electrode materials for lithium ion batteries in our group. We focus on two typical cathode materials, MoO₃ nanobelts and FeSe₂ nanoflowers. Methods of direct or secondary hydrothermal lithiation of MoO₃ nanobelts and FeSe₂ nanoflowers are described first, followed by electrochemical investigation of the samples before and after lithiation. Compared with pristine materials, lithiated samples exhibit better cycling capability. Prelithiation of other kinds of materials, such as V₂O₅, MnO₂, etc. is also briefly reviewed. This demonstrates that prelithiation can be a powerful general approach for improving cycling performance of Li-ion battery electrode materials.

I. INTRODUCTION

Li-ion and Li batteries for portable electronic devices and hybrid electric vehicles have gained tremendous importance for powering society today.^{1–3} However, how to prepare cathode materials with higher energy density and/or power density as well as longer cycle life is still a challenge. Extensive research efforts are presently devoted to overcoming these problems by doping,⁴ conductive polymers,⁵ and carbon coatings,⁶ but adding conductive polymers will make the battery less stable in higher temperature and carbon coating will lower the volumetric energy density. Prelithiation is considered an effective way to increase cycling stability of cathode and/or anode materials as well as to investigate structural changes of the electrode materials during lithium ion insertion/extraction. Johnson et al.⁷ found that lithiated MnO₂ materials prepared by reaction of α -MnO₂ with LiOH·H₂O exhibited a more stable structure and higher capacity on cycling than the parent MnO₂ material. The lithiated samples showed excellent coulombic efficiency from the first cycle (98.9%) and better capacity retention rate after 10 cycles (80.2%), compared with the parent samples (75%, 68.4%). Garcia et al.⁸ prepared Li_xV₂O₅ phase by chemical lithiation of V₂O₅ using n-butyllithium. They reported the new behavior and attractive properties of Li_{1.16}V₂O₅ electrodes aged for a few days in air.

A specific capacity of 300 mAh/g is available in the range of 1.8–3.8 V after the 20th cycle, which represents an improvement of 15%–20% compared with V₂O₅. In addition to cathode materials, prelithiation of anode materials also results in improved cycling stability. Landi et al.⁹ reported that electrochemical prelithiation of the carbon nanotube (CNT) anodes to 5 mV (versus Li/Li⁺) prior to battery assembly can improve cyclability of CNT battery. Zhang et al.¹⁰ prepared lithiated cobalt phosphides by high-energy ball milling stoichiometric amounts of Li₃N powder and the synthesized phosphide sample. Compared with the parent sample, the first cycle efficiency reached 95% for lithiated sample, and the irreversibility compensation was realized. However, the lithiated sample provided a low capacity. A possible reason for it was that the LiP phase formed by ball milling was mostly inactive toward a further lithium uptake due to massive structure defects. Seong et al.¹¹ revealed that a large initial irreversible capacity of carbon-coated silicon monoxide could be drastically reduced by a lithiation method. After lithiation, coulombic efficiency for the initial charge–discharge stage was increased from 67.7% to 72.8%. It is predicted that controlling the amount of lithium used in the prelithiation stage or enhancing lithiation reaction will dramatically improve the reversible capacity of the materials.

Among all of the cathode materials, layered vanadium and molybdenum oxides^{12–20} have the potential to offer much higher capacities, but are limited by fast capacity fading. Recently, compared with bulk/microsized

^{a)}Address all correspondence to this author.

e-mail: mlq@cmliris.harvard.edu
DOI: 10.1557/JMR.2010.0196

materials, nanostructured cathodes or anodes have a short Li-ion insertion/extraction distance and very large surface-to-volume ratio to contact with electrolyte, which can improve the cycling performance.^{21–24} In this review, we focus on prelithiation of MoO₃ nanobelts^{25,26} and FeSe₂ nanoflowers²⁷ by hydrothermal reaction, which enables better capacity retention rate during the cycling. In addition, we introduce prelithiation of other materials, such as V₂O₅ and MnO₂, and so forth.

II. METHODS OF CHEMICAL LITHIATION

Hydrothermal process is usually considered one of the effective routes to synthesize high-quality one-dimensional nanomaterials, such as nanowires, nanotubes, nanobelts, etc.^{28–31} Recently, we have successfully used hydrothermal reaction to realize chemical prelithiation of nanostructured cathode materials.^{25–27} Methods for lithiation of MoO₃ nanobelts and FeSe₂ nanoflowers are as follows. (i) MoO₃ nanobelts were synthesized by a hydrothermal synthesis technique, and lithiation was carried out by a secondary hydrothermal reaction with LiCl. Briefly, MoO₃·*n*H₂O sol was prepared by ion exchange of (NH₄)₆Mo₇O₂₄·4H₂O through a proton-exchange resin. Then, the sol was added into a Teflon-lined autoclave and kept at 180 °C for 4 h. After the hydrothermal reaction, the light-blue product was washed with deionized water and dried at 80 °C for 8 h. To attain the lithiated MoO₃ nanobelts, 0.20 g MoO₃ nanobelts were stirred with 0.29 g LiCl in deionized water for 2 days, and the resultant light-blue solution was transferred to a Teflon-lined autoclave and kept at 180 °C for 24 h. Next, the autoclave was left to cool down in air, and the solid precipitate was filtered out and washed with deionized water. The resulting slurry was allowed to dry at 100 °C. (ii) For simplicity, direct hydrothermal lithiation of MoO₃ nanobelts was carried out. 40 mL H₂O₂ (30%) was agitated rapidly and 4 g molybdenum powder was slowly added under water cooling until the clear orange sol was obtained; subsequently LiCl powder was added into the sol stirred for 12 h. The orange sol was directly transferred to a Teflon-lined autoclave and kept at 180 °C for 48 h, and the light blue product was obtained after drying at 80 °C for 4 h. The pristine MoO₃ nanobelts were synthesized under the same condition without adding LiCl. (iii) FeSe₂ nanoflowers can also be lithiated by secondary hydrothermal reaction. Briefly, 2.5 mmol ferrous oxalate, 25 mL of 0.1 M sodium selenosulfate solution, 5 mL of 1 M citric acid, and 25 mL of 9.1 wt% polyvinyl alcohol solution were mixed to form a homogeneous solution. Then the solution was transferred into a Teflon-lined autoclave, which was then sealed at 180 °C for 24 h, and the FeSe₂ nanoflowers were obtained. To attain the lithiated FeSe₂ nanoflowers, FeSe₂ nanoflowers and LiCl powder were

stirred in water and then kept at 180 °C for 24 h by the hydrothermal reaction.

In addition to hydrothermal lithiation by LiCl, there are some other agents used for chemical lithiation, such as BuLi, Li₂S, LiI, etc. Notably, BuLi can give nearly the same results as electrochemical lithiation and determine the full lithiation capacity of the materials.³² Several examples of compounds with the ReO₃ structure and shear structures derived from it have been lithiated using *n*-BuLi. Lithiation of ReO₃ results in two new hexagonal compositions LiReO₃ and Li₂ReO₃, which are related to cubic ReO₃ by a simple twist of the structure.³³ MnO₂ can be lithiated with *n*-butyllithium (25% mol excess) or with LiI (50% mol excess).⁷

III. CYCLING PERFORMANCE OF PRELITHIATED MATERIALS

A. Lithiated molybdenum oxide nanobelts

The peaks of the x-ray diffraction (XRD) patterns for MoO₃ nanobelts before and after lithiation via secondary hydrothermal reaction can be readily indexed to be orthorhombic MoO₃ (JCPDS No. 05-0508) as shown in Fig. 1(a). For the nonlithiated MoO₃ nanobelts, the strong intensities of (020), (040), and (060) peaks indicate the anisotropic growth of the nanostructure as well as the preferred orientation of the nanobelts on the substrate. Importantly, compared with the nonlithiated sample, there is a small shift of the (020) peak toward a lower diffraction angle for the lithiated sample. This is direct evidence of an expanded *b*-plane interlayer distance for 0.065 Å after lithiation, possibly due to the introduction of Li interstitials between the layers. The morphology and microstructure of the products were observed using scanning electron microscopy (SEM) and transmission electron microscopy (TEM). Before lithiation [Fig. 1(b)], the sample shows a long, beltlike morphology with widths of 80–400 nm and lengths of 5–10 μm, and a rectangle-like cross section is clearly visible. For the lithiated sample [Fig. 1(c)], however, the nanobelt length decreases to 2–6 μm, and some ruptured short segments with lengths of 200–400 nm are clearly seen in Fig. 1(c-1). In Fig. 1(c-2), the surface of the lithiated nanobelt is rougher than that of the nonlithiated sample, with the presence of surface nanoflakes. A selected-area electron diffraction (SAED) pattern [the inset in Fig. 1(b-3)] recorded with the incident electron beam perpendicular to the nanobelt shows the (010) pattern of α-MoO₃, and the growth direction is [001], the top/bottom surfaces being (010) and the side surfaces being (100). The formation of the dominant (010) surfaces is the result of the anisotropic structure.³⁴ Bullard and Smith³⁵ used AFM to characterize the structural evolution of the MoO₃ (010) surface during initial stage of Li⁺ intercalation. Because the interlayer spacing of Li_{*x*}MoO₃ is

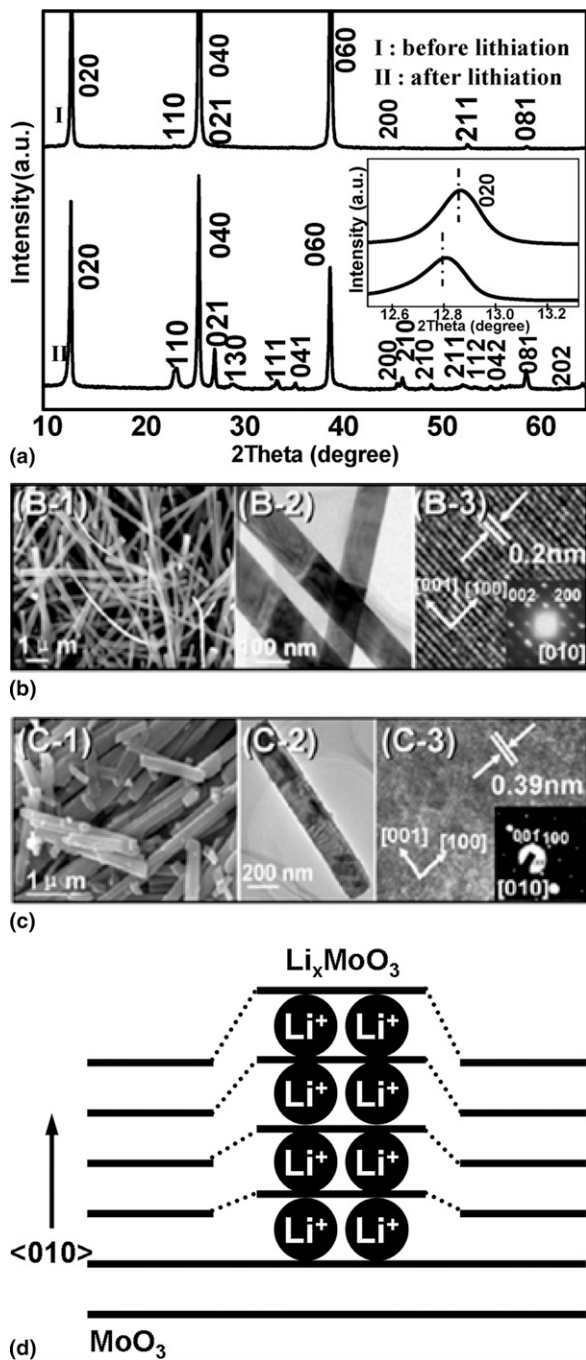


FIG. 1. (a) XRD patterns of MoO_3 nanobelts before and after lithiation via secondary hydrothermal reaction. The inset is the corresponding (020) diffraction peak. (b, c) SEM, TEM, and HRTEM characterization of the nanobelts before and after lithiation, respectively. The insets in the HRTEM images are the corresponding SAED patterns. (d) Schematic illustration of Li^+ insertion into MoO_3 layers (reprinted with permission from Refs. 25 and 35).

greater than that of MoO_3 , the Li_xMoO_3 precipitates expand out of the (010) surface as they grow into the MoO_3 crystal along [010], as shown in Fig. 1(c). This shows that lithiated MoO_3 crystals have larger b -plane

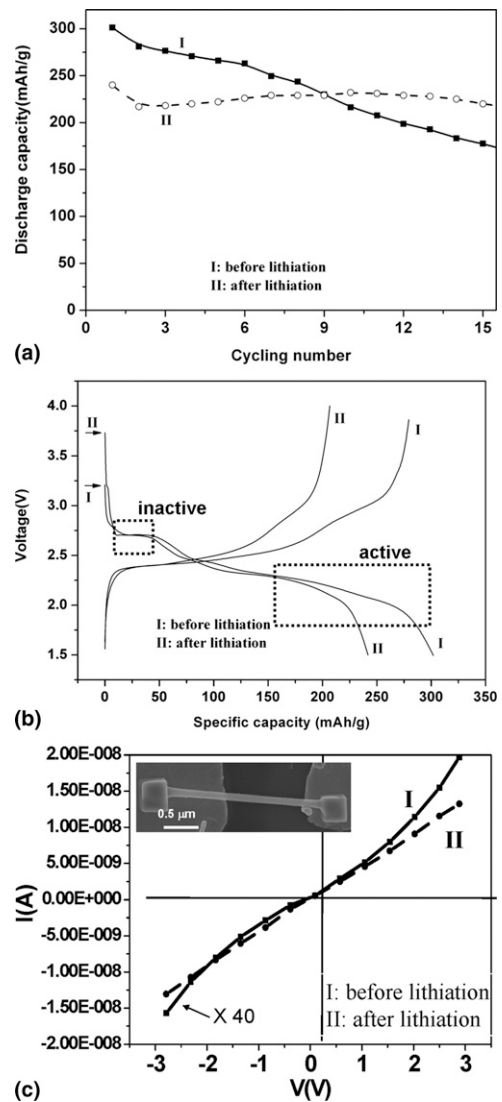


FIG. 2. (a) The discharge capacity as a function of the cycle number for the MoO_3 nanobelts before and after lithiation via secondary hydrothermal reaction. (b) Potential versus capacity curves for the first cycle of discharge-charge process of the nanobelts before and after lithiation. (c) I - V transport measurements of single nanobelt fabricated devices using the samples before and after lithiation (reprinted with permission from Ref. 25).

interlayer distance and rough surface, which is in accordance with XRD patterns and TEM images in Fig. 1.

The lithiation results in a drastic improvement in the cycling stability of the nanobelts. Figure 2(a) shows the curves of discharge capacity versus the cycle number for the nonlithiated and lithiated MoO_3 nanobelts at a current density of 30 mA/g. The discharge capacity of MoO_3 nanobelts is 301 mAh/g in the first cycle and 264 mAh/g after 5 cycles. However, the discharge capacity of bulk MoO_3 is 249 mAh/g in the first cycle and drops dramatically to 27 mAh/g after 5 cycles.³⁶ This is likely to be due to shape and size effects of the nanobelts, with increased surfaces, edges, and corners shortening

the diffusion lengths of Li ions.³⁶ We note that the lithiated MoO₃ nanobelts exhibit an initial discharge capacity slightly smaller than that of the nonlithiated MoO₃ nanobelts. Interestingly, initial discharge specific capacities of the nanobelts before and after lithiation are equal above 2.4 V, but different at 2.4–1.5 V. It is reported that lithiation of MoO₃ around 2.8 V contains irreversible structural change, and the 2.8 V plateau is not observed from the second cycle onward, but lithiation at 2.4–2.0 V is reversible.³⁷ In other words, Li⁺ ion occupied sites during lithiation at around 2.8 V are electrochemically inactive, while Li⁺ ion occupied sites during lithiation at 2.4–2.0 V are electrochemically active. Therefore, some Li⁺ ions introduced during the secondary hydrothermal lithiation process occupy some sites that are electrochemically active for Li storage, according to the first discharge curves [Fig. 2(b)] and XRD patterns [Fig. 1(a)] of the nanobelts before and after lithiation. For the nonlithiated MoO₃ nanobelts, the discharge capacity decreased to 180 mAh/g after 15 cycles, corresponding to a capacity retention of 60%. However, the discharge capacity of the lithiated MoO₃ nanobelts decreased to 220 mAh/g after 15 cycles, corresponding to a capacity retention of 92%, showing the stability and enhanced performance of the lithiated nanobelts.

To understand the superior performance of lithiated nanobelts for Li⁺ storage, we measured the electrical transport through individual MoO₃ nanobelt before and after lithiation [Fig. 2(c)]. Before lithiation, the *I*–*V* characteristics of the nanobelt show asymmetric Schottky barriers at the two ends [the solid curve in Fig. 2(c)], as created between semiconductor MoO₃ (with a band gap of 3.1 eV) and Au/Pt electrodes, and the transported current is of the order of approximately 300 pA at approximately 2 V. After lithiation, the *I*–*V* curve shows ohmic behavior [the dashed curve in Fig. 2(c)], and the transported current is of the order of 10 nA at a bias of approximately 2 V. This result suggests that the Li⁺ ions introduced during lithiation effectively converted the MoO₃ nanobelts from semiconductor to metallic behavior. According to the measured resistance, the effective length, and cross section of the nanobelt, the conductivity was evaluated to be approximately 10^{−4} and 10^{−2} S/cm before and after lithiation, respectively. Therefore, the conductivity was increased by close to 2 orders of magnitudes via lithiation. Because the nanobelt grows along [001], the increase of conductivity along the nanobelt implies an increase of carrier density in the MoO₆ octahedral layers. This suggests that Li⁺ ions have been introduced as interstitials into the layers. During the electrochemical cycling, interlayer spacing of MoO₃ continues to be widened/narrowed because of lithium ion insertion/extraction reaction. Compared with nonlithiated samples, lithiated MoO₃ nanobelts with wider interlayer spacing exhibit reduced volumetric change in

the charge–discharge process. Therefore, lithiation can enhance structural stability of MoO₃ electrode during lithium ion insertion/extraction process. The Li⁺ ions, first introduced during lithiation and later remaining in the lattice, enhance the electrical conductivity, which may assist the transport of the Li⁺ ions to be inserted and extracted in future charge–discharge processes. Cui group³⁸ investigated lithiation of single V₂O₅ nanoribbon by BuLi and found that the intrinsic conductivity of individual Li_xV₂O₅ nanoribbon is 0.001 S/cm, 3 orders magnitude lower than for pristine V₂O₅ nanoribbon. This lowered conductivity and increased contact resistance may be the result of mixed phases acting as barriers to efficient electron conduction or changes in local electronic structure. According to conductivity change of V₂O₅ or MoO₃ before and after lithiation, we can estimate that prelithiation would enhance the conductivity of lithiated samples with only one phase, in which there are no barriers caused by mixed phases.³⁹

In addition to secondary hydrothermal lithiation, we have investigated direct hydrothermal lithiation of MoO₃ nanobelts. The XRD pattern of lithiated MoO₃ nanobelts is compared with that of pristine nanobelts in Fig. 3(a). Both samples can be indexed to α-MoO₃ (JCPDS No. 05-0508). Compared with the pristine nanobelts, the increase of relative intensity of (110) and (021) peaks shows that lithiation has certain influence on the crystallization of MoO₃ nanobelts, but the lack of appearance of new peaks confirms that the crystal structure is still

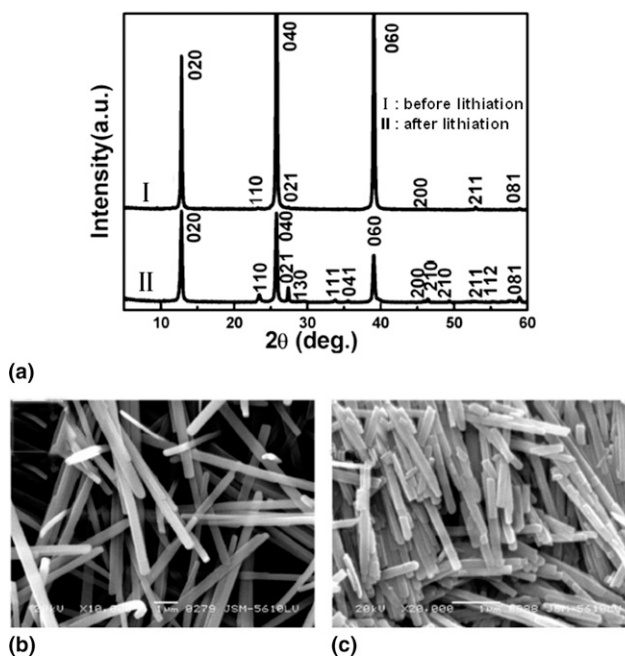


FIG. 3. (a) XRD patterns of MoO₃ nanobelts before and after lithiation via direct hydrothermal reaction. (b, c) SEM images of the nanobelts before and after lithiation, respectively (reprinted with permission from Ref. 26).

kept as orthorhombic phase. Notably, lithiation by this method does not expand the interlayer spacing, which is different from the previous report.⁴⁰ Although the radius discrepancy between Li^+ (60 pm) and Mo^{6+} (62 pm) is not remarkable, it is difficult for Li^+ ions to replace Mo^{6+} ions because of the difference in ion valence, so probably the Li^+ ions had incorporate into the interstitial sites of MoO_3 lattice. Figures 3(b) and 3(c) show SEM images of the nanobelts before and after lithiation, respectively. Lithiation has no influence on beltlike morphology, and the rectangular cross sections are visible. However, the width around ~ 200 nm is smaller than that of pristine nanobelts, and the length also decreases to 5 to 8 μm , and some fracture nanobelts with lengths of 200 to 400 nm can be seen clearly.

Figure 4 shows the curves of discharge capacity versus the cycle number for the electrodes made from pristine and lithiated MoO_3 nanobelts at charge–discharge current density of 30 mA/g. It is apparent that the discharge capacity of pristine MoO_3 nanobelts decreases greatly with cycling, fading from 301 mAh/g in the first cycle to 81 mAh/g in the 39th cycle, corresponding to capacity retention of 26.5%. Although the discharge capacity of lithiated MoO_3 nanobelts is 266 mAh/g in the first cycle, it still retains 133 mAh/g after 39 cycles, corresponding to about 50% of its first capacity. The discharge capacity of the lithiated MoO_3 nanobelts becomes lower probably because Li^+ ions had occupied some space of the interstitial sites during the hydrothermal reaction. The intercalation of Li^+ ions into MoO_3 nanobelts significantly enhances the cycling stability and reversibility; probably the Li^+ ions that occupy the interstitial site of MoO_3 layer stabilize the structure and reduce the electrostatic interaction between MoO_3 layer and Li^+ ions in interlayer during the discharge.²⁶

B. Lithiated ferroselite nanoflowers

To further investigate the effects of chemical prelithiation on cycling performance of cathode materials,

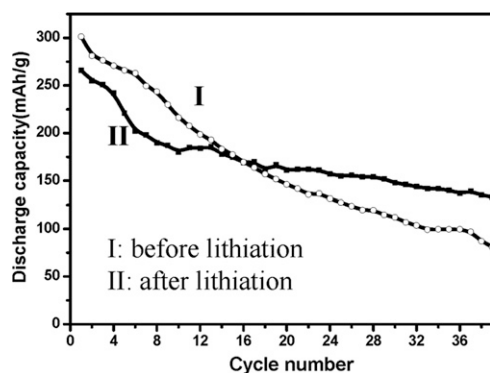
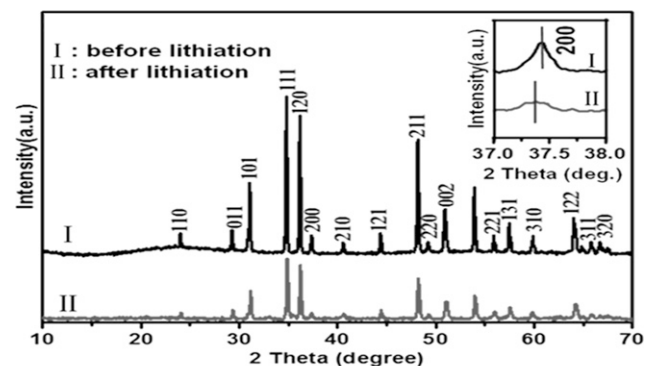


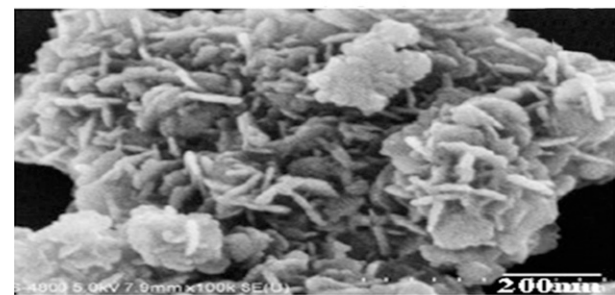
FIG. 4. Cycling property of pristine MoO_3 nanobelts and directly lithiated MoO_3 nanobelts (reprinted with permission from Ref. 26).

we have selected the typical semiconductor FeSe_2 as another example. Notably, Fe-based compounds are more advantageous as electrode materials for lithium ion batteries because iron is abundant, inexpensive, and environmentally friendly.^{41–43} Figure 5(a) shows the XRD patterns of the FeSe_2 nanoflowers before and after lithiation. All the diffraction peaks can be indexed to FeSe_2 (JCPD No. 82-0269). Notably, compared with the nonlithiated sample, a small shift of the (200) peak toward a lower diffraction angle can be observed for the lithiated sample, as shown in the inset of Fig. 5(a). This result shows an expanded a -plane interlayer distance after lithiation, which is possible because of the introduction of Li interstitials. Field emission scanning electron microscopy (FESEM) image [Fig. 5(b)] of the as-prepared FeSe_2 nanoflowers reveals that the nanoflowers are composed of uniform nanoplates about 20 nm thick and 100 nm in diameter.

Figure 6 exhibits the curves of discharge capacity versus the cycle number for the FeSe_2 nanoflowers before and after lithiation at a current density of 40 mA/g. For the nonlithiated FeSe_2 nanoflowers, the first discharge and the second discharge capacities reach 431 and 382 mAh/g, respectively, with a large irreversible capacity of about 49 mAh/g in the first cycle. For the lithiated FeSe_2 nanoflowers, a smaller irreversible capacity of about 36 mAh/g in the first cycle is observed. After 25 cycles, the discharge capacity of the nonlithiated



(a)



(b)

FIG. 5. (a) XRD patterns of FeSe_2 nanoflowers before and after lithiation. (b) FESEM image of the as-prepared FeSe_2 nanoflowers (reprinted with permission from Ref. 27).

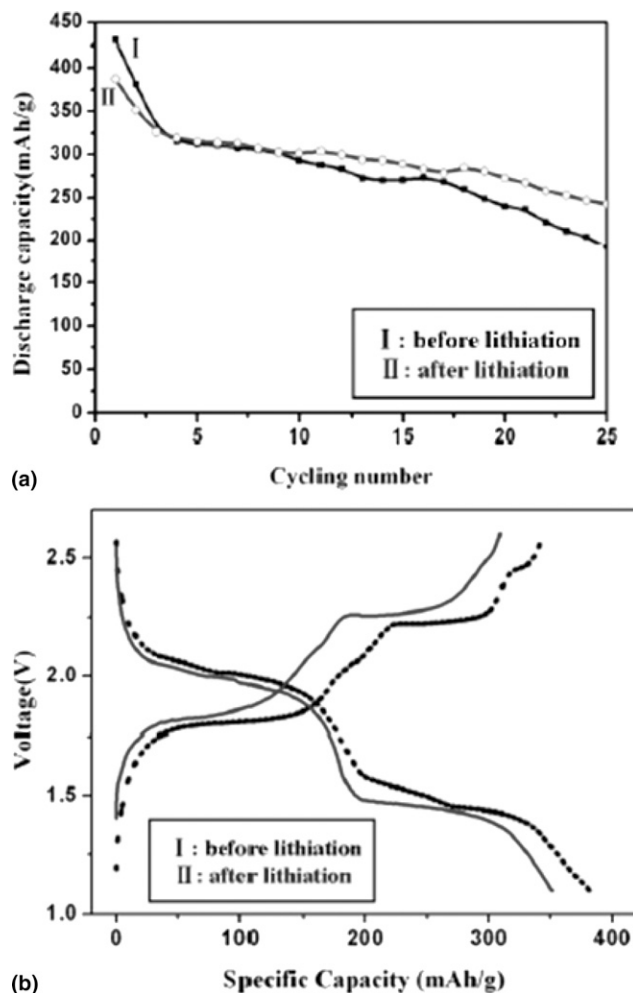


FIG. 6. (a) The discharge capacity as a function of the cycle number for the FeSe₂ nanoflowers before and after lithiation. (b) Potential versus capacity curves for the second cycle of charge–discharge process of the nanoflowers before and after lithiation (reprinted with permission from Ref. 27).

FeSe₂ nanoflowers decreases to 192 mAh/g, corresponding to a capacity retention of 45%. However, for the lithiated FeSe₂ nanoflowers, the discharge capacity decreases to 242 mAh/g after 25 cycles, corresponding to a capacity retention of 63% and showing the enhancement of cycling performance of the lithiated nanoflowers. Figure 6(b) is the potential versus capacity curve of the second cycles for the nonlithiated and lithiated FeSe₂ nanoflowers, showing the lithiated FeSe₂ nanoflowers exhibiting a lower initial discharge capacity than that of the nonlithiated FeSe₂ nanoflowers. According to XRD data in Fig. 5(a), we can deduce that some Li⁺ ions introduced during the secondary hydrothermal lithiation process have occupied some space of the interstitial sites that are electrochemically active for Li storage. The preintercalation of Li⁺ ions into FeSe₂ nanoflowers significantly enhances the cycling stability and reversibility, and the Li⁺ ions that occupy the inter-

stitial site of FeSe₂ lattice stabilize the structure and reduce the electrostatic interaction between FeSe₂ layers and Li⁺ ions in interlayer during the discharge.²⁷

C. Other lithiated materials

In addition to MoO₃ and FeSe₂, prelithiation is applicable to other materials, such as layered V₂O₅, MnO₂, etc. Garcia et al.⁸ have studied chemical prelithiation of V₂O₅ and found that prelithiation greatly affected electrochemical properties of V₂O₅. Li_xV₂O₅ compounds were obtained by chemical lithiation of V₂O₅ powder by n-butyllithium solution (1.6 M in hexane) added in stoichiometric proportions, under argon atmosphere. The reaction is described as:



Three Li_xV₂O₅ compounds, Li_{0.9}V₂O₅, Li_{1.16}V₂O₅, and Li_{1.6}V₂O₅, were prepared. For all the three lithiated samples, in the first charge process, deinsertion of Li⁺ ions was not complete. Two possibilities can explain this result. First, some lithium ions by prelithiation can be “trapped” in the lattice. Second, a chemical oxidation of Li_xV₂O₅ compounds by oxygen could explain the lower faradaic yield found during the charge process. During the subsequent discharge, the amount of Li⁺ ions inserted in the lithiated material is almost the same as that in the parent oxide. Interestingly, cycling stability is dependent on aging time for lithiated samples. After 20 cycles, the specific capacity is about 280–300 mAh/g for the 11 and 48 day aged samples against 250 mAh/g for the freshly lithiated Li_{1.16}V₂O₅ and the V₂O₅ oxide, showing an improvement of 15%–20% of the capacity. This improvement is ascribed to an increase in the reversible capacity of the third and fourth steps of the cycling. A change of the morphology and/or the structure associated with the chemical oxidation and leading to an amorphous compound could explain the better cycle life obtained.

Li and Pistoia^{44,45} reported the comparison of the behavior of cathodes based on pure and lithiated manganese oxides. They found that prelithiated samples formed from HNO₃-treated manganese oxides and LiNO₃ (7:3 molar ratio) at 370 °C showed an especially satisfactory cycling behavior. The structure of prelithiated samples was fairly resistant to lithiation and allows faster Li⁺ ion diffusion than pure MnO₂. Jung et al.⁴⁶ synthesized Li_xMnO₂ from γ-MnO₂ chemical lithiation in an aqueous solvent, in which a formaldehyde reducing agent (37% solution in water) and a lithium hydroxide (LiOH) were used. Lithiation was optimized at a molar ratio of γ-MnO₂:LiOH:HCOH = 1:4:1, which indicated a composition of $x = 0.302$ in Li_xMnO₂. Charge–discharge test showed that lithiation improved the cycling characteristics of γ-MnO₂ and achieved higher discharge capacity (265 mAh/g) than nontreated γ-MnO₂ (160 mAh/g).

IV. CONCLUSIONS

In conclusion, α -MoO₃ nanobelts and FeSe₂ nanoflowers were successfully lithiated by hydrothermal reaction while retaining their crystal structure and surface morphology. The lithiated MoO₃ nanobelts exhibited excellent cycling capability, and the conductivity of a lithiated MoO₃ nanobelt is increased by close to 2 orders of magnitudes compared with that of a nonlithiated MoO₃ nanobelt. To give another example, compared with pristine materials, capacity retention rate of lithiated FeSe₂ nanoflowers increases. Compared with pristine materials, lithiated samples exhibit better cycling capability, probably resulting from better structure stability, increased electrical conductivity, and weakening of electrostatic interaction between layers and Li⁺ ions in interlayer during the discharge process. In addition, other prelithiated materials, such as Li_xV₂O₅, Li_xMnO₂, etc. can also exhibit improved electrochemical performance compared with their parent structures. Therefore, chemical lithiated nanostructures combine the advantages of nanostructures (compared with bulk phase) and prelithiation (compared with nonlithiated samples).

ACKNOWLEDGMENTS

This work was supported by the National Nature Science Foundation of China (50702039), the Research Fund for the Doctoral Program of Higher Education (20070497012), Scientific Research Foundation for Returned Scholars, Ministry of Education of China (2008-890), and Innovation Special Foundation of Excellent Returned Scholars of Wuhan (2008-84). Thanks are due to Prof. C.M. Lieber of Harvard University, Prof. Z.L. Wang of Georgia Institute of Technology, and Prof. W. Chen of Wuhan University of Technology for strong support and stimulating discussion.

REFERENCES

- J.B. Goodenough: Cathode materials: A personal perspective. *J. Power Sources* **174**, 996 (2007).
- M. Miaomiao, N.A. Chernova, B.H. Toby, P.Y. Zavalij, and M.S. Whittingham: Structural and electrochemical behavior of LiMn_{0.4}Ni_{0.4}Co_{0.2}O₂. *J. Power Sources* **165**, 517 (2007).
- X. Ji, K.T. Lee, and L.F. Nazar: A highly ordered nanostructured carbon-sulphur cathode for lithium-sulphur batteries. *Nat. Mater.* **8**, 500 (2009).
- Y. Lee, M.G. Kim, and J. Cho: Layered Li_{0.88}[Li_{0.18}Co_{0.33}Mn_{0.49}]O₂ nanowires for fast and high capacity Li-ion storage material. *Nano Lett.* **8**, 957 (2008).
- X.H. Huang, J.P. Tu, X.H. Xia, X.L. Wang, and J.Y. Xiang: Nickel foam-supported porous NiO/polyaniline film as anode for lithium ion batteries. *Electrochem. Commun.* **10**, 1288 (2008).
- C.M. Doherty, R.A. Caruso, B.M. Smarsly, P. Adelhelm, and C.J. Drummond: Hierarchically porous monolithic LiFePO₄/carbon composite electrode materials for high power lithium ion batteries. *Chem. Mater.* **21**, 5300 (2009).
- C.S. Johnson, D.W. Dees, M.F. Mansuetto, M.M. Thackeray, D.R. Vissers, D. Argyriou, C.K. Loong, and L. Christensen: Structural and electrochemical studies of a-manganese dioxide (α-MnO₂). *J. Power Sources* **68**, 570 (1997).
- B. Garcia, M. Millet, J.P. Pereira-Ramos, N. Baffier, and D. Bloch: Electrochemical behavior of chemically lithiated Li_xV₂O₅ phases (0.99x91.6). *J. Power Sources* **68-82**, 670 (1999).
- B.J. Landi, M.J. Ganter, C.D. Cress, R.A. DiLeo, and R.P. Raffaele: Carbon nanotubes for lithium ion batteries. *Energy Environ. Sci.* **2**, 638 (2009).
- Z. Zhang, J. Yang, Y. Nuli, B. Wang, and J. Xu: CoP_x synthesis and lithiation by ball-milling for anode materials of lithium ion cells. *Solid State Ionics* **176**, 693 (2005).
- I.W. Seong, K.T. Kim, and W.Y. Yoon: Electrochemical behavior of a lithium-pre-doped carbon-coated silicon monoxide anode cell. *J. Power Sources* **189**, 511 (2009).
- L.Q. Mai, W. Chen, C.S. Jiang, Q. Xu, J.F. Peng, and Q.Y. Zhu: Effect of Mo doping and heat treatment on microstructure and electrochemical performance of vanadium oxide nanotubes, in *Continuous Nanophase and Nanostructured Materials*, edited by S. Komarneni, J.C. Parker, and J.J. Watkins (Mater. Res. Soc. Symp. Proc. **788**, Warrendale, PA, 2004), L11.36.
- Y.Y. Qi, W. Chen, L.Q. Mai, Q.Y. Zhu, and A.P. Jin: Synthesis and electrochemical performance of PEO doped molybdenum trioxide nanobelts. *Int. J. Electrochem. Sci.* **1**, 317 (2006).
- W. Chen, L.Q. Mai, Y.Y. Qi, and Y. Dai: One-dimensional nanomaterials of vanadium and molybdenum oxides. *J. Phys. Chem. Solids* **67**, 896 (2006).
- N.A. Chernova, M. Roppolo, A.C. Dillon, and M.S. Whittingham: Layered vanadium and molybdenum oxides: Batteries and electrochromics. *J. Mater. Chem.* **19**, 2526 (2009).
- L.F. Nazar, B.E. Koene, and J.F. Britten: Hydrothermal synthesis and crystal structure of a novel layered vanadate with 1,4-diazabicyclo [2.2.2]octane as the structure-directing agent: (C₆H₁₄N₂)V₆O₁₄·H₂O. *Chem. Mater.* **8**, 327 (1996).
- M.S. Whittingham: Lithium batteries and cathode materials. *Chem. Rev.* **104**, 4271 (2004).
- C. Ban, N.A. Chernova, and M.S. Whittingham: Electrospun nano-vanadium pentoxide cathode. *Electrochem. Commun.* **11**, 522 (2009).
- L.Q. Mai, W. Chen, Q. Xu, and Q.Y. Zhu: Effect of modification by poly(ethylene-oxide) on the reversibility of Li insertion/extraction in MoO₃ nanocomposite films. *Microelectron. Eng.* **66**, 199 (2003).
- L.Q. Mai, W. Chen, Q. Xu, and Q.Y. Zhu: Mo doped vanadium oxide nanotubes: Microstructure and electrochemistry. *Chem. Phys. Lett.* **382**, 307 (2003).
- L.Q. Mai, W. Chen, Y.Y. Qi, Y. Dai, and W. Jin: Synthesis and electrochemical performance of Ag-containing VONTs. *Nanosci. Technol.* **121**, 789 (2007).
- C.K. Chan, H. Peng, G. Liu, K. McIlwrath, X.F. Zhang, R.A. Huggins, and Y. Cui: High performance lithium battery anodes using silicon nanowires. *Nat. Nanotechnol.* **3**, 31 (2008).
- E. Hosono, T. Kudo, I. Honma, H. Matsuda, and H. Zhou: Synthesis of single crystalline spinel LiMn₂O₄ nanowires for a lithium ion battery with high power density. *Nano Lett.* **9**, 1045 (2009).
- C.K. Chan, X.F. Zhang, and Y. Cui: High capacity Li ion battery anodes using Ge nanowires. *Nano Lett.* **8**, 307 (2008).
- L.Q. Mai, B. Hu, W. Chen, Y.Y. Qi, C.S. Lao, R.S. Yang, Y. Dai, and Z.L. Wang: Lithiated MoO₃ nanobelts with greatly improved performance for lithium batteries. *Adv. Mater.* **19**, 3712 (2007).
- L.Q. Mai, B. Hu, Y.Y. Qi, Y. Dai, and W. Chen: Improved cycling performance of directly lithiated MoO₃ nanobelts. *Int. J. Electrochem. Sci.* **3**, 216 (2008).

27. L.Q. Mai, Y. Gao, J.G. Guan, B. Hu, L. Xu, and W. Jin: Formation and lithiation of ferroselite nanoflowers as high-energy Li-ion battery electrodes. *Int. J. Electrochem. Sci.* **4**, 755 (2009).
28. L.Q. Mai, C.S. Lao, B. Hu, J. Zhou, Y.Y. Qi, W. Chen, E.D. Gu, and Z.L. Wang: Synthesis and electrical transport of single-crystal $\text{NH}_4\text{V}_3\text{O}_8$ nanobelts. *J. Phys. Chem. B* **110**, 18138 (2006).
29. L.Q. Mai, W.L. Guo, B. Hu, W. Jin, and W. Chen: Fabrication and properties of VO-based nanorods. *J. Phys. Chem. C* **112**, 423 (2008).
30. W. Chen, L.Q. Mai, Y.Y. Qi, W. Jin, T. Hu, W.L. Guo, Y. Dai, and E.D. Gu: One-dimensional oxide nanomaterials through rheological self-assembling. *Key Eng. Mater.* **336**, 2128 (2007).
31. L. Zheng, Y. Xu, D. Jin, and Y. Xie: Novel metastable hexagonal MoO_3 nanobelts: Synthesis, photochromic, and electrochromic properties. *Chem. Mater.* **21**, 5681 (2009).
32. M.S. Whittingham and M.B. Dines: N-Butyllithium—An effective, general cathode screening agent. *J. Electrochem. Soc.* **124**, 1387 (1977).
33. D.W. Murphy, M. Greenblatt, R.J. Cava, and S.M. Zahurak: Topotactic lithium reactions with ReO_3 related shear structures. *Solid State Ionics* **5**, 327 (1981).
34. S.T. Wang, Y.G. Zhang, X.C. Ma, W.Z. Wang, X.B. Li, Z.D. Zhang, and Y.T. Qian: Hydrothermal route to single crystalline $\alpha\text{-MoO}_3$ nanobelts and hierarchical structures. *Solid State Commun.* **136**, 283 (2005).
35. J.W. Bullard and R.L. Smith: Structural evolution of the MoO_3 (010) surface during lithium intercalation. *Solid State Ionics* **160**, 335 (2003).
36. W. Chen, Y.Y. Qi, L.Q. Mai, Q. Xu, H.X. Liu, and X.J. Zhao: Hydrothermal synthesis and electrochemical behavior of MoO_3 nanobelts for lithium batteries, in *Proceedings of the 10th Asian Conference on Solid State Ionics* (World Scientific Publishing, Singapore, 2006), p. 833.
37. T. Tsumura and M. Inagaki: Lithium insertion/extraction reaction on crystalline MoO_3 . *Solid State Ionics* **104**, 183 (1997).
38. C.K. Chan, H. Peng, R.D. Twisten, K. Jarausch, X.F. Zhang, and Y. Cui: Fast, completely reversible Li insertion in vanadium pentoxide nanoribbons. *Nano Lett.* **7**, 490 (2007).
39. K.T. Lee, W.H. Kan, and L.F. Nazar: Proof of intercrystallite ionic transport in LiMPO_4 electrodes (M = Fe, Mn). *J. Am. Chem. Soc.* **131**, 6044 (2009).
40. P.A. Christian, J.N. Carides, F.J. DiSalvo, and J.V. Waszczak: Molybdenum oxide cathodes in secondary lithium cells. *J. Electrochem. Soc.* **127**, 2315 (1980).
41. Y.H. Huang and J.B. Goodenough: High-rate LiFePO_4 lithium rechargeable battery promoted by electrochemically active polymers. *Chem. Mater.* **20**, 7237 (2008).
42. A.K. Padhi, K.S. Nanjundaswamy, and J.B. Goodenough: Phospho-olivines as positive-electrode materials for rechargeable lithium batteries. *J. Electrochem. Soc.* **144**, 1188 (1997).
43. J. Chen, M.J. Vacchio, S. Wang, N. Chernova, P.Y. Zavalij, and M.S. Whittingham: The hydrothermal synthesis and characterization of olivines and related compounds for electrochemical applications. *Solid State Ionics* **178**, 1676 (2008).
44. L. Li and G. Pistoia: Secondary Li cells. I. A comparison of the behavior of cathodes based on pure and lithiated manganese oxides. *Solid State Ionics* **47**, 231 (1991).
45. L. Li and G. Pistoia: Secondary Li cells. II. Characteristics of lithiated manganese oxides synthesized from LiNO_3 and MnO_2 . *Solid State Ionics* **47**, 241 (1991).
46. W.I. Jung, M. Nagao, C. Pitteloud, A. Yamada, and R. Kann: Synthesis of Li_xMnO_2 by chemical lithiation in an aqueous media. *J. Power Sources* **195**, 3328 (2010).